19th Brazilian Congress of Thermal Sciences and Engineering
November 06th-10th, 2022, Bento Gonçalves - RS - Brazil

ENC-2022-0198
IMPACT OF COLD HEAT PIPES ON THE NUCLEAR ENERGY CONVERSION SYSTEM MASS FOR SPACE POWER GENERATION

Ermerson Ferreira de Moura[1]
Guilherme Borges Ribeiro[2]
Izabela Batista Henriques[3]
Aeronautics Institute of Technology, São josé dos Campos, Brazil.
ermerson@ita.br[1], gbribeiro@ita.br[2], izabela@ita.br[3]

Abstract. *The new space age that humanity is living is constantly expanding the limit of human presence in the solar system. New missions are being planned by space agencies and private companies to take man to planets like Mars. However, for missions like this to be possible, high-efficiency power generation systems are needed. In this perspective, nuclear power generation systems are an excellent option, as they are able to supply energy for a long period in a constant way. For systems like this to become viable, high-efficiency, low-mass energy conversion systems must be used. In this scenario, the dynamic Stirling conversion cycle proves to be an excellent option. However, these systems have several components that can make them very heavy, which could prevent their application, given the need for the system to have good compactability and low mass to allow it to be launched into space. Among these components, the heat pipe-radiator assembly is the one that has the greatest participation in the size and total mass of the system, reaching more than 1/3 of the total mass. With this in mind, this work carried out a thermodynamic modeling of the Stirling cycle together with an asymmetrical heat pipe model, to evaluate the dimensional impact of low temperature heat pipes on the system total mass. With the model, it was possible to identify that the reduction of the engine cold side temperature considerably increases the system mass, due to the need to use a greater heat-pipe-radiator system. Taking into account the configuration of the cold heat pipes, it was possible to conclude that increasing the number of heat pipes provides the greatest increase in mass for the rejection system in relation to the increase in the length and diameter of the cold heat pipes. The results also indicated that an optimization between the amount of heat pipes, heat pipes diameter and length is necessary to reach an optimal value of the heat rejection system mass.*
Keywords: *heat pipes, finite-time thermodynamics, space application, stirling engine, power generation.*

1. INTRODUCTION

With the arrival of the new space age, there is a constant increase in the development of research and technologies for space exploration, especially for deep space. Within this perspective, power generation systems with high energy density are necessary due to the high energy demand of these missions (Moura et al. 2022, Fan et al. 2017, Fan et al. 2018). Currently, there are three most used sources for this application: solar, chemical, and nuclear (Moura et al. 2021a, Araújo et al. 2018). Chemical energy delivers large amounts of energy in a small instant of time being more viable for access to space, as deep space missions are long, systems with greater availability over time are needed. The generation of photovoltaic energy is shown as an alternative for the supply of power for long periods, but its application is limited to solar incidence, and for missions in inhospitable environments or further away from the sun, its use becomes unfeasible. (Araujo et al. 2018, Dai et al. 2020, Fan et al. 2017). Within this perspective, nuclear energy is one of the most promising in view of the high energy density delivered by these systems compared to chemical and solar energy, and the great availability over time without depending on environmental conditions such as photovoltaic solar energy, which allows its application to inhospitable environments far from Earth, such as missions to Jupiter and Saturn. (Moura et al. 2021b, Fan et al. 2018, Dai et al. 2019, Dai et al. 2020).

Nuclear power generation systems can be classified between static systems and dynamic systems. Static systems do not use moving parts, which increases their reliability, but their efficiency is low, not exceedingly approximately 10% (Fan et al. 2017, El-Genk et al. 2008a, El-Genk et al. 2008b, El-Genk et al. 2008b, El-Genk et al. Genk et al. 2011). Dynamic systems have an efficiency of around 25 to 30% (Ribeiro et al. 2015, Gallo et al. 2009, Juhasz et al. 2007), and require moving parts. However, for applications that demand high energy, they are the most viable options. Dynamic nuclear power generation systems have as main components the presence of a nuclear reactor (generally fast reaction with more than 90% enrichment of the fissile material) high temperature heat pipes (HHP) for heat transfer from the reactor

core to the hot part of the conversion system. The power conversion system, which can be Brayton, Stirling, or Rankine. And the heat rejection system (heat pipe-radiator assembly) by radiation.

Among the dynamic nuclear energy conversion cycles for space applications the Stirling cycle is the one that stands out the most, compared to the Brayton cycle Stirling can reach 60% of the efficiency of an ideal Carnot cycle with a temperature ratio between 2 and 3 while the Brayton cycle reaches 40% with a temperature ratio between 3 and 4 (Lee et al. 2007). The typical Stirling engine for space applications contains a heater (hot side), cooler (cold side), piston, displacer, expansion space, compression space, regenerator, casing, support structure and linear alternators (Dai et al. 2020). For space applications reliability is of extreme importance and the insertion of moving parts increases the number of failure mechanisms, within this perspective the Free Piston Stirling Engine (FPSE) in beta configuration is used for space applications (Maxwell, 2016). An FPSE is dynamically coupled to the gas, but not mechanically, with no crank mechanism in the arrangement. In the beta configuration, the engine structure is designed so that the piston and displacer are positioned on the same cylinder (Ahmadi et al. 2017). In this way, the number of moving parts is reduced, increasing the engine reliability. The working fluid commonly used is helium due to the low density, high thermal conductivity, low viscosity and high specific heat, enhancing the cycle performance (Fan et al. 2017, Dai et al. 2020).

As previously mentioned, the heat exchange present in nuclear power generation systems in space and through radiation. The assembly of heat pipes-radiator can correspond to more than 1/3 of the mass of the system and its optimization is strictly necessary for the system to have a better mass-to-power ratio. Within this perspective, this work aims to analyze the impact of the dimensional parameters of cold heat pipes (CHP) on the mass of the heat rejection system, seeking to understand what are the key variables for reducing the system mass without impairing the power and efficiency delivered.

2. THERMODYNAMIC MODEL

The thermodynamic model adopted for this work is based on the finite-time thermodynamics approach. Thus, this model deals with processes that have explicit time or rate dependencies (Andresen et al. 1996). For the thermodynamic modeling, the following assumptions are made:

- the model is steady state with prescribed time.
- the heat transfer between the reactor core and the hot heat pipes occurs by conduction.
- heat conduction leads to a heat loss between the hot side and cold side of the Stirling cycle.
- the specific heat of the working fluid is constant.
- the working fluid is modeled as an ideal gas.
- the regenerative process is imperfect, with uniform temperature distribution.

In Figure (1), a T-s diagram is displayed, detailing the heat transfer and the thermodynamic processes involved in a typical Nuclear Stirling conversion system for space applications.

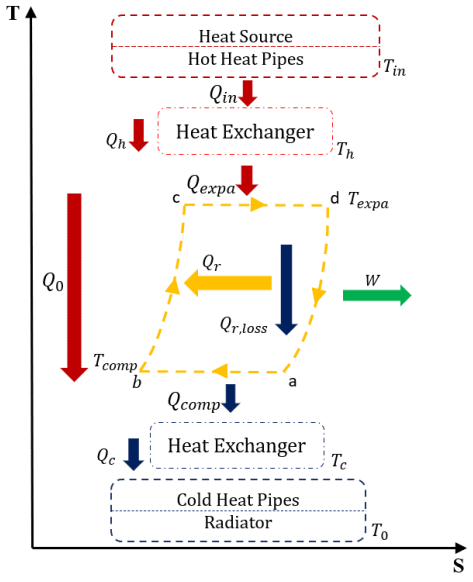

Figure 1. T-S diagram of nuclear Stirling engine with the heat flows and losses.

In this model, the temperature T_H is the difference between the temperature of the core and the temperature drop ΔT_{hp} of the hot heat pipe according to equation (1). The temperature drop calculation is obtained through a one-dimensional heat pipe model presented by Romano et al (2019, 2020, 2021) and also presented by Moura et al.(2020). In this model, the thermal conductance in each region of the heat pipe is computed, as well as the temperature drop Thus,

$$T_H = T_I - \Delta T_{hp} \tag{1}$$

This temperature drop can be obtained by calculating the resistances associated with each section of the heat pipe. A conventional heat pipe is divided into three distinct regions: the evaporating region where the heat is added, the adiabatic, and condensing where the heat is rejected. The resistances considered for this model are: the resistance of the container, the wick region, the liquid-vapor interface, and the vapor region (Romano, 2018) (Reay et al. 2014). For the container can be described as:

$$UA_{con} = \frac{1}{2\pi K_{con} L_e} ln\left(D_{con}/D_{cap}\right) \tag{2}$$

Where K_{Con} the thermal conductivity of the casing material, Le the length of the evaporating region, D_{con} and D_{cap} are the diameters of the casing and the wick region. For the wick region, can be described as:

$$UA_{cap} = \frac{1}{2\pi K_{cap} L_e} ln\left(D_{cap}/D_{va}\right) \tag{3}$$

Where D_{va} the diameter of the steam region, and K_{cap}, described according to the following equation:

$$k_{cap} = \frac{\left(w_{fin}\, k_l\, k_{ti}\, d_{gr}\right) + w_{gr}\, k_l (0.185\, w_{fin}\, k_{ti} + d_{gr}\, k_l)}{\left(w_{gr} + w_{fin}\right)(0.185\, w_{fin}\, k_{ti} + d_{gr}\, k_l)} \tag{4}$$

Where w_{fin} the length of the wick groove, k_l is the conductivity of the working fluid, k_{ti} is the conductivity of the wall thickness of the wick region, d_{gr} is the deep groove, w_{gr} is the length of the wick groove. For the resistance of the liquid-vapor interface:

$$UA_i = \frac{R\, T_{va,e}{}^2 \sqrt{2\,\pi\, R\, T_{va}}}{MW\; 2\,\pi\, L_e\, h_{lv}{}^2} \tag{5}$$

Since R the gas constant, T_{va} the temperature of the vapor in the evaporator zone, MW is the molar mass of the fluid and h_{lv} the enthalpy of vaporization of the fluid in the evaporator region. For steam region, can be described as:

$$UA_{va} = \frac{\left(P_{va,e} - P_{va,c}\right)\left(\frac{\left(T_{va,c} + T_{va,e}\right)}{2}\right)}{h_{lv,va}\, \rho_{va}\, \dot{Q}_{hp}} \tag{6}$$

Where $P_{va,e}$ and $P_{va,c}$ the saturation pressure of the fluid in the evaporator and condenser region. T_{va} is the temperature of the vaporized fluid in the evaporating and condensing region. $H_{lv,va}$ the enthalpy of steam, ρ_{va} the density of the fluid and $\dot{Q}_{hp}$ the heat flux that enters the heat pipe. To Know UA_{hp} corresponding the overall thermal conductance of the heat pipe is used:

$$\frac{1}{UA_{hp}} = \frac{1}{UA_{con,e}} + \frac{1}{UA_{cap,e}} + \frac{1}{UA_{i,e}} + \frac{1}{UA_{va}} + \frac{1}{UA_{i,c}} + \frac{1}{UA_{cap,e}} + \frac{1}{UA_{con,c}} \tag{7}$$

Where the subscript “e “corresponds to the evaporating region and “c” for condensing region. In this way, the temperature step of the heat pipe is given by:

$$\frac{\mathrm{Q_{in}}}{\mathrm{UA}_{hp}} = \Delta \mathrm{T_{hp}} \tag{8}$$

Where Q_{in} is the heat core. For the heat pipe to operate normally, the values of diameters and lengths must be respected to reach limits of its operation, which are capillary, sonic, viscous, boiling, and entrainment limits. The limits were considered for each variation in the dimensions of the heat pipe as well as the maximum capillarity pressures. To validate the equations used and simplify the operation model of the heat pipe, the vapor flow rate of its working fluid is limited to a laminar and incompressible regime (Rev <2300 and Ma <0.2, respectively). Also, for the calculation of the overall thermal conductance of cold heat pipes (CHP), the procedure is the same, just changing the input heat and the properties of the container material and working fluid (in the case of the cold heat pipes is titanium and water, respectively). For the Stirling cycle model, the thermal bridge between the hot and cold side of the Stirling engine is proportional to the temperature difference and the cycle time (τ), being described by the following equation (Fan et al. 2017).

$$Q_0 = \nu_o(T_H - T_C)\tau \tag{9}$$

where ν_o is the heat leak coefficient between the hot and cold side, and T_C is the cold side temperature. In this model, finite heat transfer through the regenerator is considered. The regenerative processes are affected by the internal thermal resistances in the regenerator. Thus, there are regenerative losses per cycle during the two regenerative processes. The regenerative heat transfer is proportional to the temperature difference of the working fluid, and can be described as (Shubhash et al. 2014):

$$Q_r = nc_v\varepsilon_r\left(T_{expa} - T_{comp}\right) \tag{10}$$

where n is the number of moles of Helium, c_v is the specific heat on a molar basis, ε_R is the efficiency of the regenerator, and T_{expa} and T_{comp} denote the expansion and compression temperatures, respectively. Considering the fractional deviation from the ideal regeneration, the heat loss Q_R in the regenerator can be described as follows (Shubhash et al. 2014):

$$Q_{r,loss} = nc_v(1 - \varepsilon_r)\left(T_{expa} - T_{comp}\right) \tag{11}$$

The convective heat transfer is assumed to be the main heat transfer mechanism between the heat exchangers and the working fluid. Thus, the amount of heat absorbed by the working fluid on the hot side and released to the cold side can be described by the following equations (Shubhash et al. 2014):

$$Q_{expa} = UA_{hc}\left(T_H - T_{expa}\right)\tau_1 = nRT_{expa}ln\lambda + nc_v(1 - \varepsilon_r)\left(T_{expa} - T_{comp}\right) \tag{12}$$

$$Q_{comp} = UA_{cc}\left(T_{comp} - T_C\right)\tau_2 = nRT_{comp}ln\lambda + nc_v(1 - \varepsilon_r)\left(T_{expa} - T_{comp}\right) \tag{13}$$

where Q_{expa} is the amount of heat absorbed by the working fluid, Q_{comp} is the amount of heat released by the working fluid, R is the universal gas constant; UA_{HC} is the thermal conductance of the hot side heat exchanger, UA_{CC} is the thermal conductance of the cold side heat exchanger; and λ is the compression ratio, being described as follows

$$\lambda = \frac{V_{comp}}{V_{expa}} \tag{14}$$

where V_{comp} is the volume of the compression side and V_{expa} is the volume of the expansion side. The periods of the processes of expansion and compression, τ_1 e τ_2, respectively, can be described as

$$\tau_1 = \frac{nRT_{expa}ln\lambda + nc_v(1 - \varepsilon_r)\left(T_{expa} - T_{comp}\right)}{UA_{hc}\left(T_H - T_{expa}\right)} \tag{15}$$

$$\tau_2 = \frac{nRT_{comp}ln\lambda + nc_v(1 - \varepsilon_r)\left(T_{expa} - T_{comp}\right)}{UA_{cc}\left(T_{expa} - T_C\right)} \tag{16}$$

The total cycle period is the sum of the time of the four processes. Thus, we have

$$\tau = \tau_1 + \tau_2 + \tau_3 + \tau_4 \tag{17}$$

where the periods τ_3 and τ_4 denotes the period of each isochoric process that occur in the regenerator. These periods can be calculated with the model presented by Dai et al. (2018) as follows

$$\tau_3 = \frac{\ln\left[1 - \left(1 + \frac{C_r}{C_f}\right)\frac{T_{expa} - T_{comp}}{T_{expa} - T_C}\right]}{-\alpha_r\left(\frac{1}{C_r} + \frac{1}{C_f}\right)} \tag{18}$$

$$\tau_4 = \frac{\ln\left[1 - \left(1 + \frac{C_r}{C_f}\right)\frac{T_{expa} - T_{comp}}{T_H - T_{comp}}\right]}{-\alpha_r\left(\frac{1}{C_r} + \frac{1}{C_f}\right)} \tag{19}$$

where C_r and C_f are the regenerator and fluid heat capacities, respectively, being $C_f = m_f c_v$, m_f is the fluid mass and c_v is the specific heat of the working fluid at constant volume. Moreover, α_r denotes the regenerator heat transfer coefficient. For this model, it will be assumed that the thermal conductivity of the regenerator is sufficiently large, allowing the temperature distribution to be uniform. The heat transfer coefficient of the working fluid and the regenerator varies with time. Thus, the regenerator effectiveness can be defined as

$$\varepsilon_r = \frac{T_{expa} - T_C}{T_H - T_C} = \frac{T_h - T_{comp}}{T_H - T_C} \tag{20}$$

The engine hot side heat is the combination of the heat from the expansion process adding the thermal bridge. And the heat from the engine cold side is the sum of the heat from the compression process plus the thermal bridge. Therefore, the equations can be described, respectively, as follows:

$$Q_H = Q_{expa} + Q_0 \tag{21}$$

$$Q_C = Q_{comp} + Q_0 \tag{22}$$

Considering the cycle period of the Stirling engine τ, the system power output $\dot{W}$ can be computed as

$$\dot{W} = \frac{W}{\tau} = N_{stg}\frac{Q_H - Q_C}{\tau} \tag{23}$$

where N_{stg} the number of Stirling engines. The cycle energy efficiency η_t is obtained as

$$\eta_t = \frac{Q_h - Q_c}{Q_h} \tag{24}$$

In this modeling, there is a coupling between the thermodynamic model mentioned above and a dynamic model that allows calculating the displacements of the piston and the displacer as a function of process time τ. However, to calculate the τ it is necessary to know the compression ratio, however, it is necessary to know the displacement of the piston and the displacer and as mentioned it is a function of the process time. Thus, to obtain a solution, both models must be solved in a coupled manner through a numerical method that allows the computation of both variables. For the sake of conciseness, further details about the dynamic modelling can be seen in the follow studies: Moura et al. (2021a,2021b,2022). Para o cálculo da massa total do sistema a seguinte expressão pode ser usada.

$$m_s = (m_{core} + m_{stg} + m_{rad})1.15 \tag{25}$$

where the m_{core} is assumed as 5.82 kg. kW^{-1} according to Fan et al. (2017), m_{stg} is the stirling mass calculate according to the dynamic model in studies aforementioned. Furthermore, an increase of 15% of the mass is considered, corresponding to the power processing and cabling Noca et al. (2001). The mass of the radiator is the combination between the cold heat pipes mass and panel mass, according to equation (26):

$$M_{rad} = M_{hp,c} + M_{pa} \tag{26}$$

The mass of the cold heat pipes can be calculated from the following equation:

$$M_{hp,c} = \left(\rho_{hp,c} V_{hp,c} + M_f\right) N_{hp,c} \tag{27}$$

where $\rho_{hp,c}$ is the density of the heat pipe material, $V_{hp,c}$ is the volume of the heat pipe and M_f is the mass of the fluid considering the phase change of the same and an additional 5% according to Vlassov et al. (2006).

3. RESULTS AND DISCUSSION

To verify the best characteristics for these systems, the following parameters will be kept constant, as seen in table 1:

Table 1. – Inputs used for the stirling cycle.

Variable	Value	References
$\dot{Q}_{In}$ (core heat)	$400\ kW$	Guimarães et al. (2019)
UA_{CC}(Hot overall Thermal conductance)	$200\ W/K$	Fan et al. (2017)
UA_{HC} (Cold overall thermal conductance)	$200\ W/K$	Fan et al. (2017)
n (mols)	$1\ mol$	Fan et al. (2017)
ε_r (regenerator effectiveness)	0.9	Fan et al. (2017)
R (Universal gas constant)	$8.314\ J/Mol.K$	Fan et al. (2017)
v_0(Heat leak coefficient)	$2.5\ W/K$	Fan et al. (2017)
c_v (Work fluid specific heat)	$12.5\ J/mol.K$	Dai et al. (2018)
T_I (Heat source temperature)	$1200\ K$	Fan et al. (2017)
T_0(Environment temperature)	$150\ K$	Author's decision
T_C (Temperature of cold side)	$300\ K$	Author's decision
α_r (Regenerator heat transfer coefficient)	$500\ W/m.K$	NASA Lewis Center (1999)
σ (Stephan-Boltzmann constant)	$5.67x10^{-8}\ W/m^2.K^4$	Siegel (1981)
ξ (Emissivity)	0.9	Siegel (1981)
t_{rad} (Radiator thickness)	$4\ mm$	Author's decision
σ_y (Yield limit)	$880\ MPa$	Haden et al. (2015)
σ_{ult} (Ultimate limit)	$950\ MPa$	Haden et al. (2015)

The temperature of the space in regions close to the earth can vary from 393 K to 100K. In this work, a fixed temperature of 150 K was defined as the environment temperature. In order to evaluate the best engine parameters, a number of 8 Stirling engines is kept fixed. For hot heat pipes, it will be considered that the container material is niobium, and the liquid metal is lithium. For the low temperature heat pipes, the metal of the container is titanium, and the working fluid is water, while the material used for the radiator panels is aluminum. The number of heat pipes on the hot side will be 150 heat pipes (based on the proportion of heat pipes in the reactor core presented by fan et al. (2017)) and the cold side 100. The values considered for the heat pipes can be seen in table (2).

Table 2. Variables used for heat pipes.

Variable	Value	References
$D_{con,h}$ (Container diameter)	$12\ mm$	Romano et al. (2018)
$D_{gr,hp,h}$ (Deep groove)	$0.3\ mm$	Romano et al. (2018)
$w_{gr,hp,h}$ (Length of the wick groove)	$0.5\ mm$	Romano et al. (2018)
$w_{fin,hp,h}$ (Length of the wick groove)	$0.5\ mm$	Romano et al. (2018)
$l_{c,hp,h}$(condensing region length)	$0.5\ m$	Romano et al. (2018)
$l_{e,hp,h}$ (evaporating region length)	$0.5\ m$	Romano et al. (2018)
$l_{a,hp,h}$ (adiabatic region length)	0	Romano et al. (2018)
$D_{con,c}$ (Container diameter)	$0.1\ m$	Romano et al. (2018)
$D_{gr,hp,c}$ (Deep groove)	$0.3\ mm$	Romano et al. (2018)
$w_{gr,hp,c}$ (Length of the wick groove)	$0.5\ mm$	Romano et al. (2018)
$w_{fin,hp,c}$ (Length of the wick groove)	$0.5\ mm$	Romano et al. (2018)
$l_{c,hp,c}$ (condensing region length)	$0.5\ m$	Romano et al. (2018)
$l_{e,hp,c}$ (evaporating region length)	$0.5\ m$	Romano et al. (2018)
$l_{a,hp,c}$ (adiabatic region length)	0	Romano et al. (2018)
$N_{hp,h}$ (number of heat pipes)	150	Fan et al. (2017)
$N_{hp,c}$ (number of heat pipes)	100	Author's decision

As discussed earlier in order for the heat pipes to operate normally the operating limits must be respected. This way, in figure (2) the heat transfer limits for the cold heat pipes (CHP), were obtained. Therefore, for the adopted configurations, the operational limits were respected. Also, can be noted that all limits, except for the capillary limit, are much higher than the current heat transfer rate transported by the pipes. These parameters were chosen because, at temperatures below 300 K, the viscous and sonic limits are very low associated with the melting point of water, which is 273.2 K. So, to be able to use water as working fluid, the heat pipe dimensions had to be oversized. The capillary limit is associated with the mass flow of the working fluid, which was limited to not exceed 2400 Reynolds numbers, for the model remain valid.

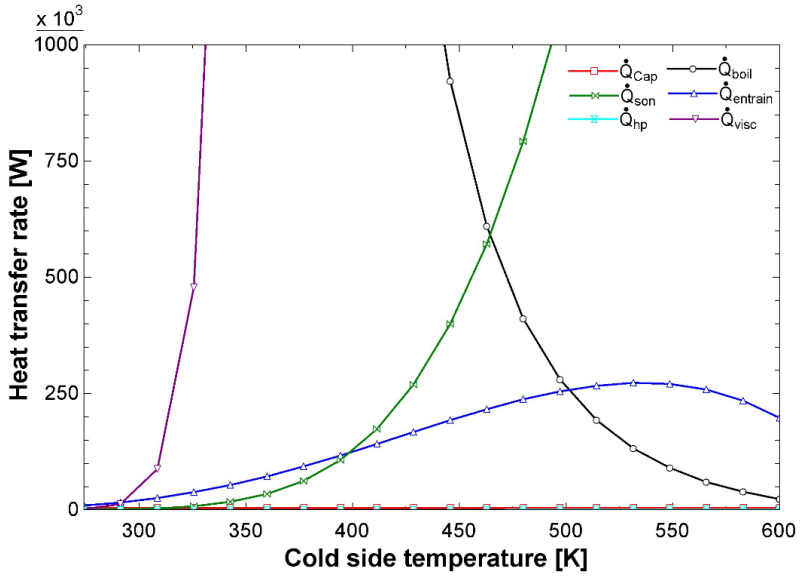

Figure 2. Cold heat pipe limits.

In figure (3a), the influence of the increase the cold side temperature on the system mass is evaluated. With the elevation in the cold side temperature, a considerable reduction in the radiator mass is seen. This reduction is more accentuated (until the temperature of 450 K). The reactor core mass and the hot heat pipes are not affected by cold side temperature, so the core and hot heat pipes mass remains constant. The Stirling engine mass and cold heat pipes increase slightly, due to the increase of cold side temperature. The increase in cold heat pipe mass also occurs due to the increases the temperature difference between the evaporating and condensing region of the CHP. In figure (3b) the mass of each component is calculated for different heat source temperatures. With the increase of heat source temperature, the Stirling engine shows slight increases of mass caused by the pressure elevation, affecting the cylinder. The radiator is the component that is more influenced by the temperature variation, being the radiator the most responsible for the system, and the panels the most massive component of the rejection system. Also note, that the mass of the system increases in the same proportion pulled by the radiator mass.

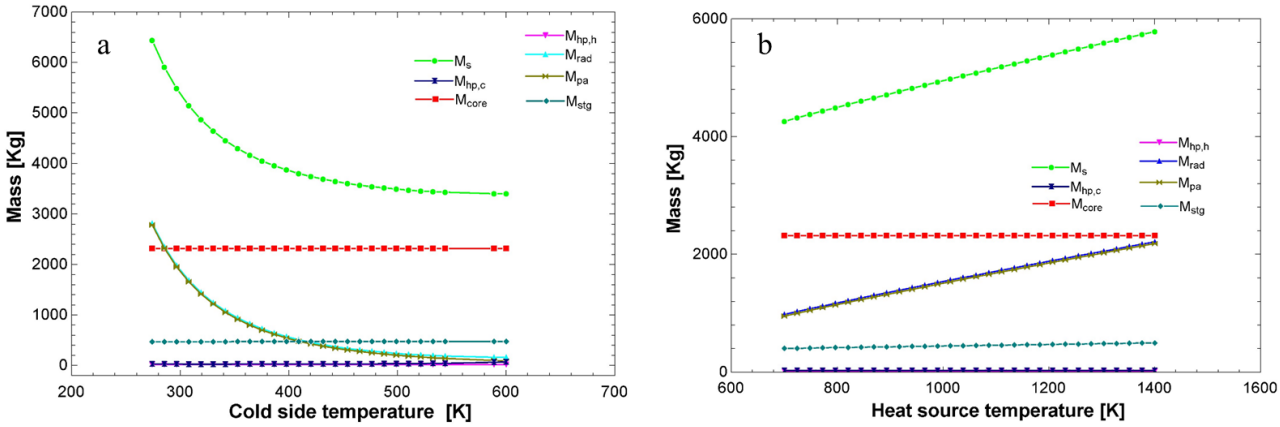

Figure 3. Mass of all system components as a function of the heat source temperature.

As confirmed by the previous result, the heat rejection system can be responsible for more than 1/3 of the entire system. So, the dimensional parameters of the CHP were varied to verify its impact on the mass of the radiator. To

calculate the mass of the radiator panel, it was considered that its thickness is a fixed value according to the table (1). In figure (4) the diameter of the cold heat pipes was varied and the impact of this increase on the mass of the radiator was verified. With an increase in diameter from 0.01 to 0.2 m the rejection system had its mass increased from 1849 kg to 1941 kg, representing an increase of 4.97% in the radiator mass.

Considering the parameters in table (2), the increase in the length of the cold heat pipes increases the system mass most than the diameter increase according to the result of the figure (5). Increasing the length from 0.5 m to 10 m, the mass of the system increases 266 kg, an increase bigger than that observed with the elevation in diameter. This increase represents 14.02% of the total rejection system mass.

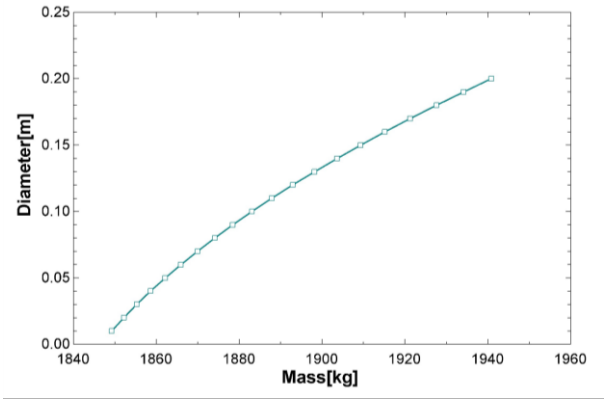

Figure 4. Diameter of heat pipe as a function of the radiator mass.

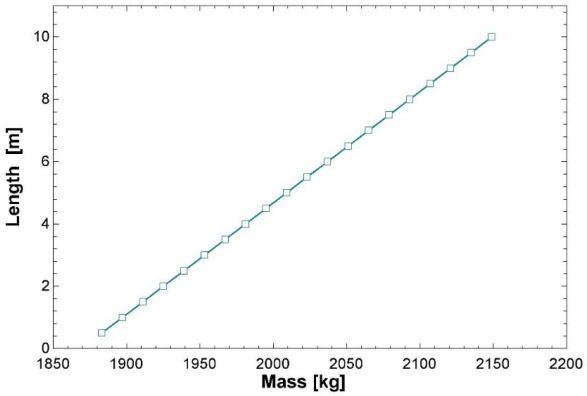

Figure 5. Length of heat pipe as a function of the radiator mass.

In figure (6) the increase of 10 heat pipes to 1000 represented an elevation of 362 kg (19.57% of the increase in the total mass) in the rejection system mass. thus, keeping the other values constant according to the table (2) the increase in the number of heat pipes is the parameter that most grows the radiator mass.

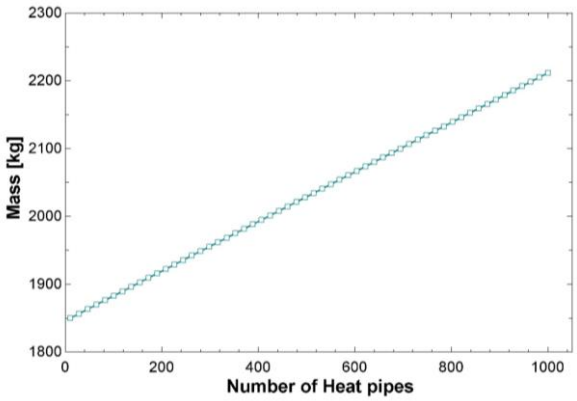

Figure 6. Radiator mass as a function of the number of cold heat pipes.

In table (3), different configurations of quantity, length, and diameter of heat pipes are compared. The configuration with the lowest mass was the configuration with the smallest number of heat pipes with the largest diameter, and the configuration with 500 pipes obtained the highest mass according to the table (3). Note, according to the results in the table presented, the component that presents the greatest mass of the rejection system is the panels, which for this work the material considered was aluminum. The use of alternative materials with lower density and with the same or better thermal conductivity can considerably reduce the heat pipe-radiator assembly mass. Considering the cold heat pipes, a correct optimization between the three parameters (Number of heat pipes, diameter, and length) is necessary to reduce the rejection system mass.

Table 3. Comparison between the heat pipes mass with different parameters.

Number of heat pipes	Diameter [m]	Mass of radiator-heat pipe assembly [kg]	Mass of the panels [kg]	Mass of heat pipes [kg]
10	0.2	1774	1768	6.04
50	0.15	1796	1774	21.84
100	0.1	1801	1773	28.07
500	0.05	1843	1775	67.65
1000	0.012	1798	1766	31.78

4. CONCLUSION

In the present work, a finite-time thermodynamic modeling was performed to analysis nuclear-powered Stirling engine for space power generation. From the model developed, it was possible to identify the increase in diameter has the least impact on the overall mass of the system, when compared to the increase in quantity and length. The configuration with fewer HPs of larger dimensions has less impact on the mass. However, the panels have the greatest mass on the rejection system and the optimization of the panels using advanced materials can provide great gains for the power system energy density for space applications. In this way, the area of the panel has a great impact on the system mass.

In this sense, and evaluating the results obtained, this study carried out to evaluate cold heat pipes from a nuclear power generation cycle to space can provide valuable insights for the study and development of power cycles for this application. In this way, this study can serve as an initial guide for evaluation of the initial configurations of cold side heat pipes coupled to the power cycle heat rejection system for space nuclear power generation, providing a parametric study in relation to various dimensional parameters of this component.

5. REFERENCES

1. Ahmadi, M. H., Ahmadi, M.-A., Pourfayaz, F. “Thermal models for analysis of performance of Stirling engine: A review”. Renewable and Sustainable Energy Reviews, 68, (2017) 168–184. doi:10.1016/j.rser.2016.09.033.
2. Ahmadi M.H, Sayyaadi H., Dehghani S., Hosseinzade H. “Designing a solar powered Stirling heat engine based on multiple criteria: maximized thermal efficiency and power”. Energy Convers. Manage 75 (2013) 282–291.
3. Andresen, B. “Finite-time thermodynamics and thermodynamic length”. Revue Générale de Thermique. 35(418-419), 1996, 647–650.
4. Araújo E.F, Guimarães L.N.F. “American Space Nuclear Electric Systems”. J Aerosp Technol Manag. (2018) 10:e4418.
5. Berchowitz D. M. “A Phasor Description of the Stirling Cycle”. The International Stirling Engine Conference (ISEC 2016) Available in: < https://www.ohio.edu/mechanical/stirling/ISEC_papers/ISEC2016-Berchowitz.pdf> Access in: 05/11/2020
6. Dai D.D, Yuan F., Long R., Liu Z.C., Liu W. “Imperfect regeneration analysis of Stirling engine caused by temperature differences in regenerator”. Energy Conversion and Management 158 (2018) 60–69.
7. Dai, Z., Wang, C., Zhang, D., Tian, W., Qiu, S., Su, G.H. “Thermoelectric characteristics analysis of thermionic space nuclear power reactor”. International journal of energy research, 2019, vol 4.
8. Dai Z., Wang C., Zhang D., Tian W., Qiu S., Su G.H. “Design and analysis of a free-piston stirling engine for space nuclear power reactor”. Nuclear Engineering and Technology (2020).
9. De Moura E.F., Ribeiro G.B., Henriques I. B. “Thermodynamic Analysis of a Stirling Cycle for Space Power Systems”. 18th Brazilian Congress of Thermal Sciences and Engineering, Virtual conference, 2020.
10. De Moura E.F., Henriques I. B., Ribeiro G.B. “Thermodynamic Modeling and Exergy Analysis of a Stirling Cycle for Space Power Generation”. ECOS 2020 - The 33rd International Conference on Efficiency, Cost, Optimization, Simulation and Environmental Impact of Energy Systems June 29-July 3, 2020, Osaka, Japan.
11. De Moura E.F., Henriques I.B., Ribeiro G.B. “Coupling of Finite Time Thermodynamic-Dynamic Models of a Stirling Engine for Nuclear Space Propulsion”. 26 ABCM International Congress of Mechanical Engineering, November 22-26, 2021. Florianopolis, SC, Brazil.

12. De Moura E.F., Henriques I.B., Ribeiro G.B., “Finite-Time Thermodynamics and Exergy Analysis of a Stirling Engine for Space Power Generation, Thermal Science and Engineering Progress”, (2021), doi: https://doi.org/10.1016/j.tsep.2021.101078.
13. De Moura E.F., Henriques I.B., Ribeiro G.B. “Thermodynamic-Dynamic coupling of a Stirling engine for space exploration” Thermal Science and Engineering Progress”, (2022), doi: https://doi.org/10.1016/j.tsep.2022.101320.
14. El-Genk M.S. “Space nuclear reactor power system concepts with static and dynamic energy conversion”. Energy Convers. Manage 49 (2008a) 402–411
15. El-Genk M.S. “Space reactor power systems with no single point failures”. Nucl.Eng. Des. 238 (2008b) 2245–2255.
16. El-Genk M.S, Schriener. T.M. “Long operation life reactor for lunar surface power”. Nucl. Eng. Des. 241 (2011) 2339–2352.
17. Fan S.;Li M.; Li S.; Zhou T.; Hu Y.; Wu S. “Thermodynamic analysis and optimization of a stirling cycle for lunar surface nuclear power system”. Applied Thermal Engineering 111 (2017) 60-67.
18. Fan S. , Hu, Y., Li M. , Li S. , Zhou T. “Thermodynamic performance of lunar surface nuclear power system with heat sink temperature change in a rotational period”. Applied Thermal Engineering 130 (2018) 127–134
19. Feng W., Lingen C., Fengrui S., Jiuyang Y. “Performance Optimization of Stirling Engine and Cooler Based on Finite-Time Thermodynamic”. Chemical Industry Press, Beijing, 2008.
20. Gallo, B. M.; El-Genk, M. S. “Brayton rotating units for space reactor power systems”. Energy Conversion and Management. v. 50, n. 9, p. 2210–2232, 2009.
21. Ribeiro G.B., Filho F.A.B., Guimarães L.N.F. “Thermodynamic analysis and optimization of a closed regenerative Brayton cycle for nuclear space power systems”. Appl. Therm. Eng. 90 (2015) 250–257
22. Guimarães, L. N. F. “TERRA Project Update (2019), A Brazilian Nuclear Space Microreactor Development”. International Nuclear Atlantic Conference –INAC 2019 XXIth Meeting on Nuclear Reactor Physics and Thermal Hydraulics –XXI ENFIR Santos, SP October 23rd, 2019
23. Haden, C. V., Collins, P. C., & Harlow, D. G. “Yield Strength Prediction of Titanium Alloys”. JOM, 67(6), 2015 1357–1361.
24. ISO 9809-1. “Gas cylinders - Refillable seamless steel gas cylinders - Design, construction and testing - Part 1: Quenched and tempered steel cylinders with tensile strength less than 1 100 MPa”.
25. Juhasz, A. “Heat Transfer Analysis of a Closed Brayton Cycle Space Radiator”. 5th International Energy Conversion Engineering Conference and Exhibit (IECEC), n. June, p. 25–27, 2007
26. Kwankaomeng S., Silpsakoolsook B., Savangvong P. “Investigation on Stability and Performance of a Free-Piston Stirling Engine”. 2013 International Conference on Alternative Energy in Developing Countries and Emerging Economies, 2013.
27. Lee S. M. , Jeffrey G. S. “Historical Review of Brayton and Stirling Power Conversion Technologies for Space Applications”. NASA/TM—2007-214976
28. Liao T., Lin J. “Optimum performance characteristics of a solar-driven Stirling heat engine system”. Energy Convers. Manage 97 (2015) 20–25.
29. Maxwell H.B. “Improving Free-Piston Stirling Engine Power Density”. NASA/TM—2016-219144
30. Reay D. A., Kew P. A., Mcglen R. J. Heat pipes. 6th. ed. Amsterdam: Elsevier, 2014
31. Romano, L. F. R., Ribeiro, G. B. Parametric evaluation of a heat pipe-radiator assembly for nuclear space power systems. Thermal Science and Engineering Progress, 2019, 100368.
32. Romano, L. F. R., Ribeiro, G. B. Cold-side temperature optimization of a recuperated closed brayton cycle for space power generation. Thermal Science and Engineering Progress, 2020, 100498.
33. Romano, L. F. R., Ribeiro, G. B. Optimization of a heat pipe-radiator assembly coupled to a recuperated closed Brayton cycle for compact space power plants. Applied Thermal Engineering, 2021, 117355.
34. Shubhash C. Kaushik ;Sudhir K.; Tyagi; Pramod Kumar. Finite Time Thermodynamics of Power and Refrigeration Cycles. Springer 1st ed, 2017.
35. Yaqi L., Yaling H., Weiwei H. “Optimization of solar-powered Stirling heat engine with finite-time thermodynamics”. Renew. Energy 36 (2011) 421–427.
36. Zohuri, B. “Heat Pipe Design and Technology”. (2016) doi:10.1007/978-3-319-29841 -2.

6. RESPONSIBILITY NOTICE

The Authors are the only responsible for the printed material included in this paper.